



Auto Disturbance Rejection Control Strategy of Wind Turbine Permanent Magnet Direct Drive Individual Variable Pitch System Under Load Excitation

Lianchao Sheng¹ · Min Li^{2,3} · Yueqi Li¹ · Wei Li²

Received: 15 July 2020 / Revised: 15 December 2020 / Accepted: 23 January 2021 / Published online: 15 February 2021
© The Korean Institute of Electrical Engineers 2021

Abstract

The wind turbine blades have complex stress states, and the load has the characteristics of time-varying and uncertainty. Aiming at the interference problem caused by complex and variable load characteristics to the individual pitch control system, combined with the variable-pitch load characteristics, based on the permanent magnet synchronous motor (PMSM) vector control strategy and LADRC (Auto Disturbance Rejection Speed Controller), an individual pitch speed controller is designed. Linear expansion state observer is built. The control algorithm is deduced and the relationship between each control parameter is analyzed to improve the anti-interference ability of the system to the abrupt load of the pitch. On this basis, the system position tracking controller is built. Finally, a vector control simulation model was built based on MATLAB/Simulink, and a speed control simulation was carried out. The simulation results show that LADRC has a strong anti-load disturbance capability, and has better anti-disturbance resistance than PID speed control, and the position controller based on this has a better position tracking effect. At the same time, the effectiveness of the designed independent pitch speed controller has also been verified through experiments. It is of great significance for improving the conversion efficiency of wind energy.

Keywords Individual variable pitch · PMSM · Auto disturbance rejection speed controller · State observer

1 Introduction

Wind energy is receiving more and more attention as a reusable clean energy source. With the construction and advancement of a low-carbon clean, efficient and safe modern energy system, the health status of wind turbines [1, 2] and their wind energy conversion efficiency become particularly important. Among them, the blade control is closely related to the conversion efficiency of wind energy. At present, the blade control has also experienced fixed pitch stall control, to unified variable pitch control, and then to the current mainstream individual pitch control [3, 4]. Individual pitch

control, as the most commonly used method, is designed to smooth the output power of wind turbines [5, 6] and reduce the cyclic load of wind turbine blades, towers and other components [7]. The individual variable pitch control system, as one of the three major control systems for wind turbines, is responsible for stabilizing the output power of the wind turbine and suppressing the vibration of blades, towers and other components. To improve the reliability of the individual pitch and reduce its failure rate, it is necessary to explore integrate scientific issues of the wind turbine's individual pitch system including the driving components, transmission structure, control system and other elements.

PMSM and its speed regulation technology have been widely used in wind turbines [8, 9], equipment manufacturing [10, 11], electric vehicles [12, 13] and marine ships [14]. Therefore, a new direct-drive variable-pitch transmission structure driven by a PMSM is proposed in this paper. The permanent magnet direct drive system has the advantages of high efficiency, energy saving, high power density, simple transmission chain, flexible regulation, low vibration and low noise [15, 16], which can effectively reduce the failure rate of the individual pitch drive system. Vector control

✉ Lianchao Sheng
shenglianchao@163.com

¹ School of Mechatronic Engineering, Jiangsu Normal University, Xuzhou 221116, China

² School of Mechatronic Engineering, China University of Mining and Technology, Xuzhou 221116, China

³ Jiangsu Jinling Intelligent Manufacturing Research Institute Co., Ltd, Nanjing 210001, China

is currently the most commonly used control scheme for PMSM. Based on vector control, the three closed-loop control structure in the PMSM position control system [17] has one more speed closed loop than the commonly used double closed-loop structure. The speed closed loop improves the accuracy of speed regulation, so the three closed loop structure is more suitable for the pitch control system that requires movement trajectory. PMSM position servo control has many control objects. The system model, load torque, etc. have an important influence on the control accuracy. Because the wind turbine blade load is relatively special, its control method is somewhat different from the common position control. At present, many scholars have conducted research in the field of individual pitch control strategies. E. A. Bossanyi [18] for the first time formally proposed a method for suppressing blade vibration using individual pitch control, thus starting the study of individual pitch control. Sandquist et al. [19] proposed an individual pitch controller based on the concept of multivariate linear quadratic Gaussian to reduce the load of megawatt wind turbines. The simulation results show that IPC control is more effective in reducing blade load. Liu et al. [20] proposed a vibration reduction strategy for large-scale variable-speed wind turbines based on pitch control and torque control. Ren et al. [21] designed an extended order and disturbance observer to estimate and compensate unknown time-varying nonlinearities and disturbances, and studied a pitch controller based on nonlinear PI. Van et al. [22] proposed an advanced pitch angle control strategy based on fuzzy logic for variable speed wind turbines. The output power and speed of the generator is used as the control input variables of the fuzzy logic controller. To overcome the uncertainty of wind turbine modeling and wind speed curve, Asgharnia et al. [23] proposed two advanced controllers, called fuzzy PID and fractional fuzzy PID, to improve the performance of pitch control. Yin et al. [24] proposed a variable displacement pump-controlled pitch system to mitigate load fluctuations in wind turbine generator power and flap direction. Lasheen A et al. [25] introduced the design of discrete-time L_1 adaptive controller for centralized pitch control of variable-speed variable-pitch wind turbines. In the reference [26], a new adaptive control strategy was developed for pitch control of wind turbines. In addition, the current sliding mode control [27, 28], adaptive control of nonlinear system [29–31] can also provide reference for individual pitch system. Although there are many researches on independent pitch control, few of them consider the actual operation characteristics of load. On the other hand, most of the current research is still using double closed-loop control.

On the basis of existing research, to further improve the reliability and stability of the individual pitch system, combined with the load characteristics of the pitch, a variable-pitch transmission structure directly driven by a PMSM is

proposed, and a three-closed-loop position control system that meets the requirements of variable-pitch control, especially the speed loop, is designed. The permanent magnet direct drive individual variable pitch control method is proposed. The linear auto disturbance rejection controller and the extended state observer are constructed. The permanent magnet direct drive individual variable pitch control simulation platform and experiment platform were built to explore the individual variable pitch control performance of the wind turbine directly driven by the PMSM. The control effect of the designed speed controller is verified. The research results are of great significance for improving the performance of individual pitch control, improving its dynamic performance, and improving the reliability of the individual pitch system. The individual variable-pitch transmission system of the wind turbine directly driven by the PMSM is shown in Fig. 1, which eliminates the reduction gear between the motor and the actuator.

2 Mathematical Modeling of PMSM

The mathematical model of PMSM must be established before the speed anti-interference controller and state observer are built. PMSM belongs to a complex system of multivariable, strong coupling, nonlinear and time-varying under the stator coordinate axis system. During the operation of PMSM, the stator and rotor are always in relative motion state. Permanent magnet and winding, winding and winding influence each other. The electromagnetic relationship is very complex. Coupled with nonlinear factors such as magnetic circuit saturation, it is very difficult to establish an accurate mathematical model of PMSM. To simplify the mathematical model of PMSM, it is idealized and is derived based on the following assumptions [16]. (1) Ignoring motor

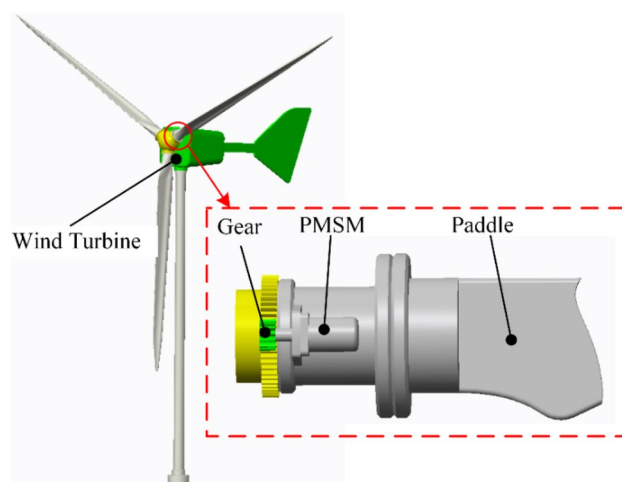


Fig. 1 Individual variable pitch drive system driven by PMSM

core saturation and parameter changes; (2) Inductance changes sinusoidally with rotor position; (3) Stator winding magnetomotive force is symmetrical sinusoidal.

Therefore, the three-phase winding voltage equation of the PMSM in the three-phase stationary coordinate system can be expressed as,

$$\begin{bmatrix} u_a \\ u_b \\ u_c \end{bmatrix} = \begin{bmatrix} R_s & 0 & 0 \\ 0 & R_s & 0 \\ 0 & 0 & R_s \end{bmatrix} \begin{bmatrix} i_a \\ i_b \\ i_c \end{bmatrix} + \frac{d}{dt} \begin{bmatrix} \psi_a \\ \psi_b \\ \psi_c \end{bmatrix} \quad (1)$$

where u_a 、 u_b 、 u_c are the phase voltages of the three-phase winding; R_s is the stator phase winding resistance; i_a 、 i_b 、 i_c are the current of the three-phase winding; ψ_a 、 ψ_b 、 ψ_c are the flux linkage of the three-phase winding.

The calculation formula of three-phase winding flux linkage of PMSM is,

$$\begin{bmatrix} \psi_a \\ \psi_b \\ \psi_c \end{bmatrix} = \begin{bmatrix} L_{aa} & M_{ab} & M_{ac} \\ M_{ba} & L_{bb} & M_{bc} \\ M_{ca} & M_{cb} & L_{cc} \end{bmatrix} \begin{bmatrix} i_a \\ i_b \\ i_c \end{bmatrix} + \psi_f \begin{bmatrix} \cos \theta_e \\ \cos(\theta_e - 2/3\pi) \\ \cos(\theta_e + 2/3\pi) \end{bmatrix} \quad (2)$$

where L_{aa} 、 L_{bb} 、 L_{cc} are the self-inductances of the three-phase winding; M_{ab} is the mutual inductance between the A-phase and B-phase, and the other mutual inductance variable symbols have similar meanings; ψ_f is the flux linkage of the permanent magnet; θ_e is the electrical angle of the rotor, that is, the angle between the rotor flux ψ_f and the A-phase winding.

According to the principle of electromechanical energy conversion, the electromagnetic torque T_e is equal to the partial derivative of the magnetic field energy storage to the mechanical angular displacement θ_m , so there is,

$$T_e = \frac{1}{2} p_n \frac{\partial}{\partial \theta_m} (i_a \psi_a + i_b \psi_b + i_c \psi_c) \quad (3)$$

where p_n is the number of pole pairs of the PMSM; The relationship between θ_m and θ_e is $\theta_e = p_n \theta_m$.

According to Newton's second law, the motion equation of the system is,

$$J_m \frac{d^2 \theta_m}{dt^2} + B_m \frac{d\theta_m}{dt} + T_L = T_e \quad (4)$$

where J_m is the rotational inertia of the system. B_m is the viscous friction coefficient of the system, and T_L is the load torque.

The relationship between the input, state and output of the mathematical model in the stator coordinate system is intricate, and the mathematical model in the stator coordinate system is difficult to apply to the dynamic analysis of PMSM. To this end, the coordinate transformation method can be used to transform the physical quantities such as voltage, current, inductance, and flux linkage

into a rotating coordinate system, so that the three-phase stator winding is equivalent to a virtual two-phase synchronous rotating winding to realize the excitation current and torque current decoupling. After decoupling, the magnetic flux and torque of the PMSM can be individually controlled, that is, vector control. For the convenience of controller design, according to the relationship between the dq coordinate system and the ABC coordinate system, the coordinates are changed, and the voltage equation in the $d-q$ coordinate system is obtained as,

$$\begin{bmatrix} u_d \\ u_q \end{bmatrix} = \begin{bmatrix} R_s + L_d \frac{d}{dt} & -\omega_e L_q \\ \omega_e L_d & R_s + L_q \frac{d}{dt} \end{bmatrix} \begin{bmatrix} i_d \\ i_q \end{bmatrix} + \begin{bmatrix} 0 \\ \omega_e \psi_f \end{bmatrix} \quad (5)$$

where u_d 、 u_q are the voltage of the straight axis and the cross axis respectively; ω_e is the electrical angular velocity of the rotor; L_d 、 L_q are the inductance of the straight axis and the cross axis respectively.

The electromagnetic torque equation in the $d-q$ coordinate system is,

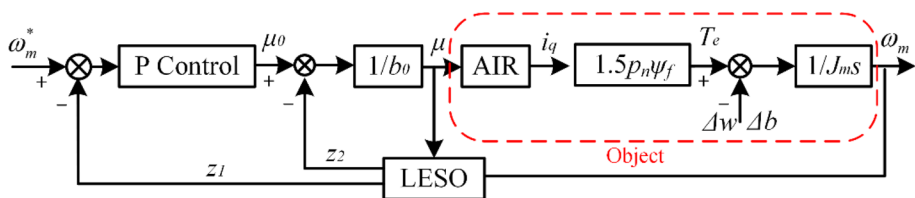
$$T_e = \frac{3}{2} p_n i_q [i_d (L_d - L_q) + \psi_f] \quad (6)$$

3 Linear Auto Disturbance Rejection Speed Control Strategy

In order to run smoothly, a reasonable anti-interference control strategy must be established. The external input wind speed of the wind turbine is uncertain. Its actual value often deviates from the test value, so the observation of the load torque becomes particularly difficult. The disturbance of the permanent magnet direct drive variable pitch system will have a greater impact on the stable operation of the speed loop. Therefore, to improve the anti-disturbance capability and robustness of the speed control system, while taking into account the simplicity of the controller and the requirement of small calculation, linear auto-disturbance control (LADRC) is adopted to realize the speed control in the three closed-loop control structure.

The LADRC system is composed of a linear controller and a linear expansion state observer (LESO). Proportional control can be used as a linear controller, as shown in Fig. 2. The electromagnetic time constant of the PMSM is much smaller than the mechanical time constant of the system motor. The sampling frequency of the current loop is higher than the sampling frequency of the speed loop, so the current loop can be regarded as an ideal controllable current source, that is, the tracking error of i_q is not considered.

Fig. 2 LADRC speed control block diagram



3.1 State Observer Design

LESO is designed first. LESO is the core part of LARDC for uncertain systems. It can be used to observe the state variables and estimate the real-time values of the uncertainties and disturbances of the system model, and then convert the real-time values of the uncertainty and disturbance values of the system model into the extended state of the system. The low order differential signal is obtained by the integral of high order differential signal by using the method of extended dimension integral. The noise signal is greatly suppressed by integral processing. The state variables and their differential values of the system can be observed effectively by LESO. The information can be transmitted to the controller to realize the system stability control.

According to the motion Eq. (4), the first-order motion equation under uncertain load can be described as,

$$\dot{\omega}_m = -a_0\omega_m + w + bi_q \tag{7}$$

where input and output are i_q and ω_m , $w = -T_L/J_m + \Delta w$, $b = 1.5p_n\psi_f/J_m + \Delta b$, $a_0 = B_m/J_m$; Δw 、 Δb are external unknown disturbances introduced by parameter perturbations such as T_L 、 B_m 、 ψ_f .

The actual unknown total disturbance is defined as,

$$f' = w + \Delta bi_q \tag{8}$$

To retain the information of known objects, the model of known objects is extended to disturbances. The sum of the unknown total disturbance f' and the known object $-a_0\omega_m$ is defined as the extension of the disturbance.

$$f = -a_0\omega_m + f' \tag{9}$$

Therefore, Eq. (7) can be written as,

$$\dot{\omega}_m = f + b_0i_q \tag{10}$$

where b_0 is the known part, and $b_0 = 1.5p_n\psi_f/J_m$.

The system disturbance f is expanded into the state variables of the system, so that Eq. (7) can be transformed into the second-order expanded state equation of the object model.

$$\begin{cases} \dot{x} = Ax + Bu + Ef' \\ y = Cx \end{cases} \tag{11}$$

where $u = i_q$, $x = \begin{bmatrix} \omega_m \\ f \end{bmatrix}$, $A = \begin{bmatrix} 0 & 1 \\ -a_0 & 0 \end{bmatrix}$, $B = \begin{bmatrix} b_0 \\ 0 \end{bmatrix}$, $E = \begin{bmatrix} 0 \\ 1 \end{bmatrix}$, $C = [1 \ 0]$. In the state equation of the objectless model $A = \begin{bmatrix} 0 & 1 \\ 0 & 0 \end{bmatrix}$. In contrast, state equations with object models are more informative.

The model-assisted second-order linear expansion state observer corresponding to Eq. (7) is as follows,

$$\begin{cases} \dot{z} = [A-LC]z + [B,L]u_c \\ y_c = z \end{cases} \tag{12}$$

where $z \rightarrow x$, $z = [z_1 \ z_2]^T$ is the observed state vector; L is the observer error feedback gain matrix to be designed, $L = [l_1 \ l_2]^T$; y_c is the output of the observer; $u_c = [u \ y]^T$ is the input of the observer.

To simplify the design process of LESO, through parameterization, the poles of the characteristic equation of the observer characteristic matrix $[A-LC]$ are placed at the same position $-\omega_0$. Let the characteristic polynomial of the observer satisfy,

$$s^2 + l_1s + l_2 = (s + \omega_0)^2 \tag{13}$$

Thus, we can get, $l_1 = 2\omega_0$, $l_2 = \omega_0^2$.

3.2 Controller Design

Then the linear controller is designed. The estimation error of z_2 is ignored, that is $z_2 \rightarrow f$. Thus, the system can be reduced to a first-order integral system,

$$\dot{y} = (f - z_2) + u_0 \approx u_0 \tag{14}$$

A simple proportional controller can be used to control u_0 .

That is,

$$u_0 = k_{sp}(\omega_m^* - z_1) \tag{15}$$

where ω_m^* is the given value of speed. k_{sp} is the parameter of P controller to be designed.

Through the simultaneous Eqs. (10) and (11), the final control signal expression can be obtained as,

$$u = \frac{u_0 - z_2}{b_0} \tag{16}$$

The parameters l_1, l_2 are reduced to a parameter ω_0 after parameterization, which simplifies the tuning of the gain matrix. Theoretically, the controller can be quickly adjusted through a single adjustment of K_{sp} . b_0 is calculated using the parameters of the system, but in order to improve the control effect, b_0 can also be adjusted appropriately according to the actual situation. The convergence speed of LADRC control can be adjusted by K_{sp}, b_0 and ω_0 . It is found that ω_0 has the most obvious effect in debugging. Larger ω_0 can accelerate the convergence speed, but it will also increase overshoot.

4 Permanent Magnet Direct Drive Variable Pitch Control Simulation

To verify the effectiveness of the control method, the system is simulated. The variable-pitch load of wind turbines [19, 24] is uncertain, and there is a large sudden load during the pitch process. Therefore, it is necessary to verify the step response performance of the drive system to the sudden load. Based on the principle of vector control, the speed control simulation model was built using Matlab/Simulink, as

shown in Fig. 3. The resistance of the PMSM is $R_s = 4.95\Omega$. The inductance of the straight axis is $L_d = 149\text{mH}$. The inductance of the cross axis is $L_q = 180\text{mH}$. The value of the rotor flux linkage is 8.7Wb , and the LADRC control module is shown in Fig. 4.

The total duration of the LADRC control simulation is 0.5 s. The SVPWM switching frequency is 5 kHz. The target speed of the PMSM is set to 15r/min. The motor is started with no load, and a step load with an amplitude of 1000 N m is applied at 0.2 s. To analyze the performance of LADRC speed control, LADRC speed control is compared with PI

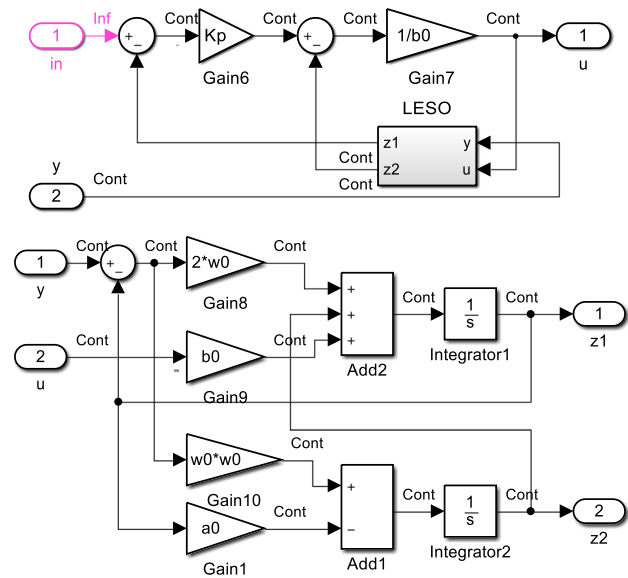


Fig. 4 LADRC control module

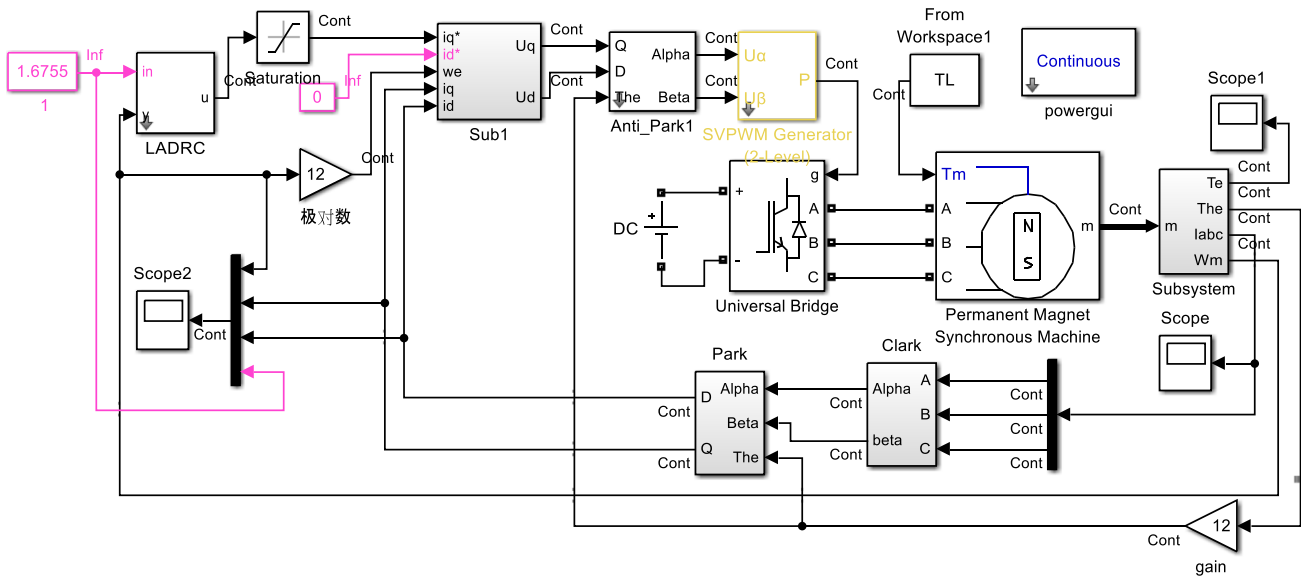


Fig. 3 LADRC speed control simulation model

speed control. The parameters of the LADRC controller are set to $K_{sp} = K_p = 20,000$, $b_0 = 22$, $\omega_0 = 110$, $a_0 = 0.9$, and the speed and current response curves of the motor are drawn as shown in Fig. 5. Due to the sudden step load disturbance at 0.2 s, the motor speed suddenly dropped by 30%, and then returned to the target value after about 0.1 s. Compared with PI control, LADRC control has stronger anti-abrupt load disturbance ability. It can be seen from the Fig. 5 that the cross-axis and straight-axis current tracking response is fast and the error is small. The target current i_q^* of the cross-axis almost overlaps with the actual current curve i_q . Only at the starting time, due to the limitation of the motor current loop bandwidth, there is a lag in the cross-axis current tracking phenomenon.

On the basis of the speed control simulation model, a position controller with feed forward control is added to form a PMSM synchronous vector control simulation model, as shown in Fig. 6, and the control effect of the position controller under individual pitch load changes is simulated.

Because the driving modes of the three blades are consistent and symmetrical, this section takes the pitch angle

of one of the blades following the control process as the research object. Assuming that the initial value of the pitch angle of the wind turbine is 0° , the pitch control is started due to the increase in wind force. The blade moves to the 5° position, and then the individual pitch control is performed. The duration of this simulation is set to 6 s. During the first 1 s, the blades are driven from 0° to 5° . The latter 5 s is the individual pitch control. The entire process limits the pitch angle adjustment speed to no more than $10^\circ/\text{s}$. In the variable pitch drive structure, the number of teeth of the large gear is 108 teeth, and the number of teeth of the small gear is 11 teeth. Regardless of the gear transmission error and transmission power loss, the target rotation angle curve and the motor load curve of this simulation are calculated according to the transmission ratio, and the rotation angle and speed change curves of the simulation process are drawn as shown in Fig. 7.

The curves in Fig. 7 can be returned. After the motor moves to the specified position at a constant speed, it starts to follow the target rotation angle. Even at the moment of sudden torque change, the actual rotation angle maintains

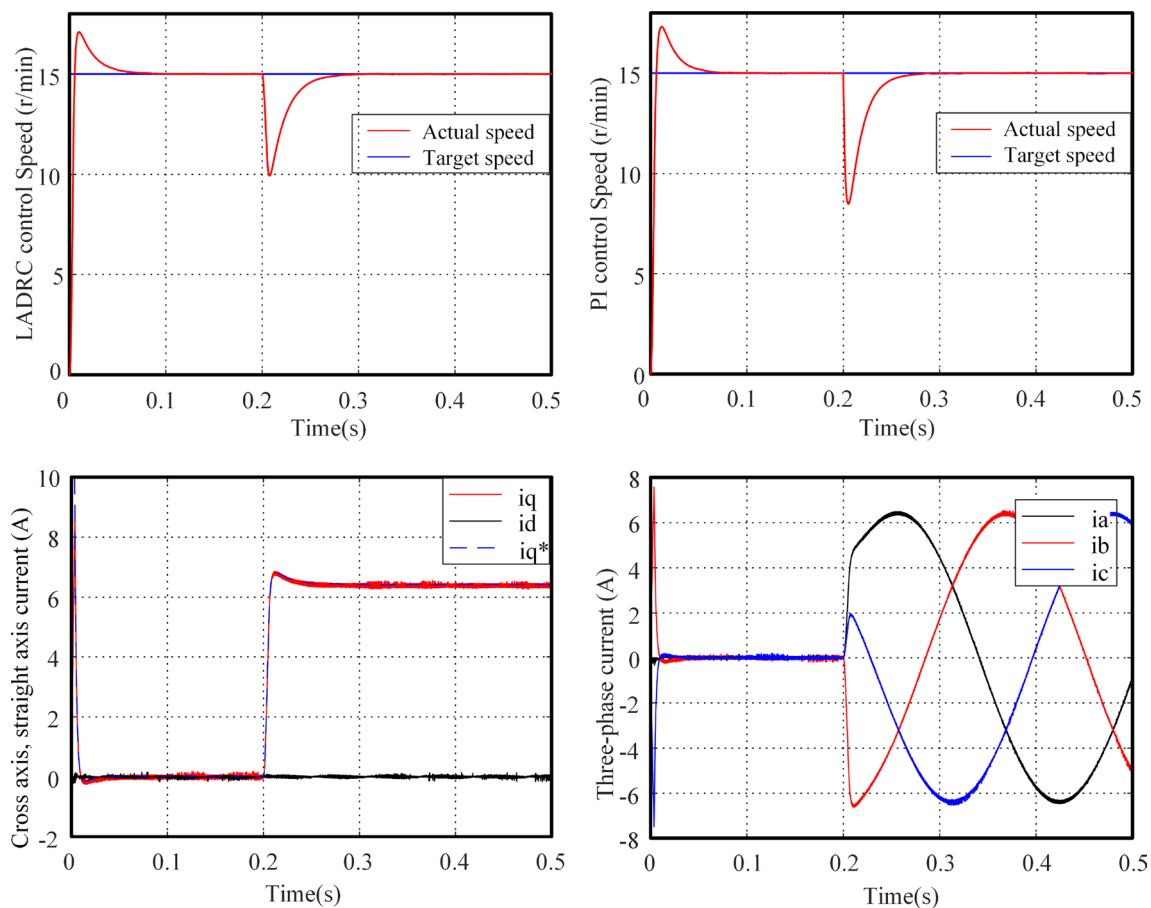


Fig. 5 Speed and current response curves of speed control simulation

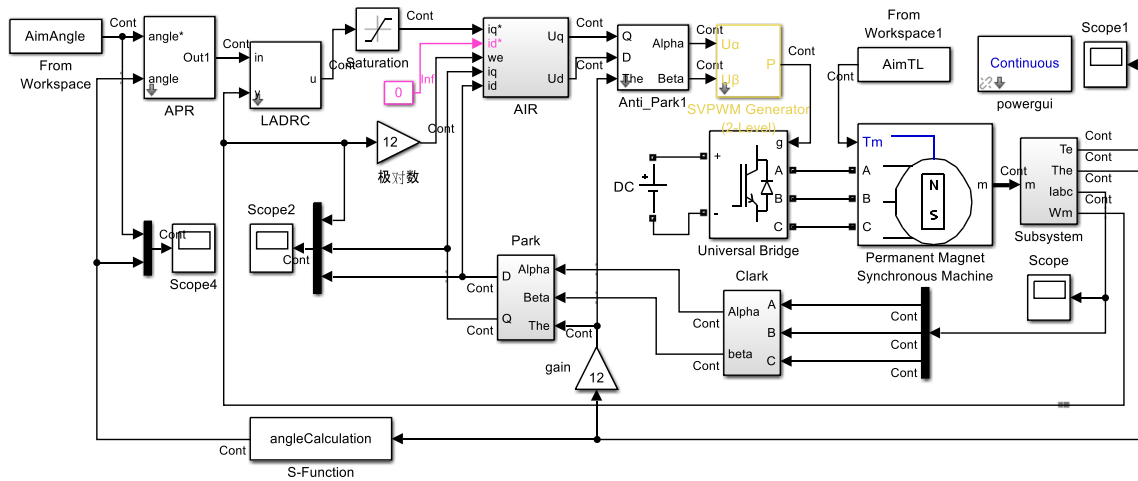


Fig. 6 Pitch angle position following control simulation model

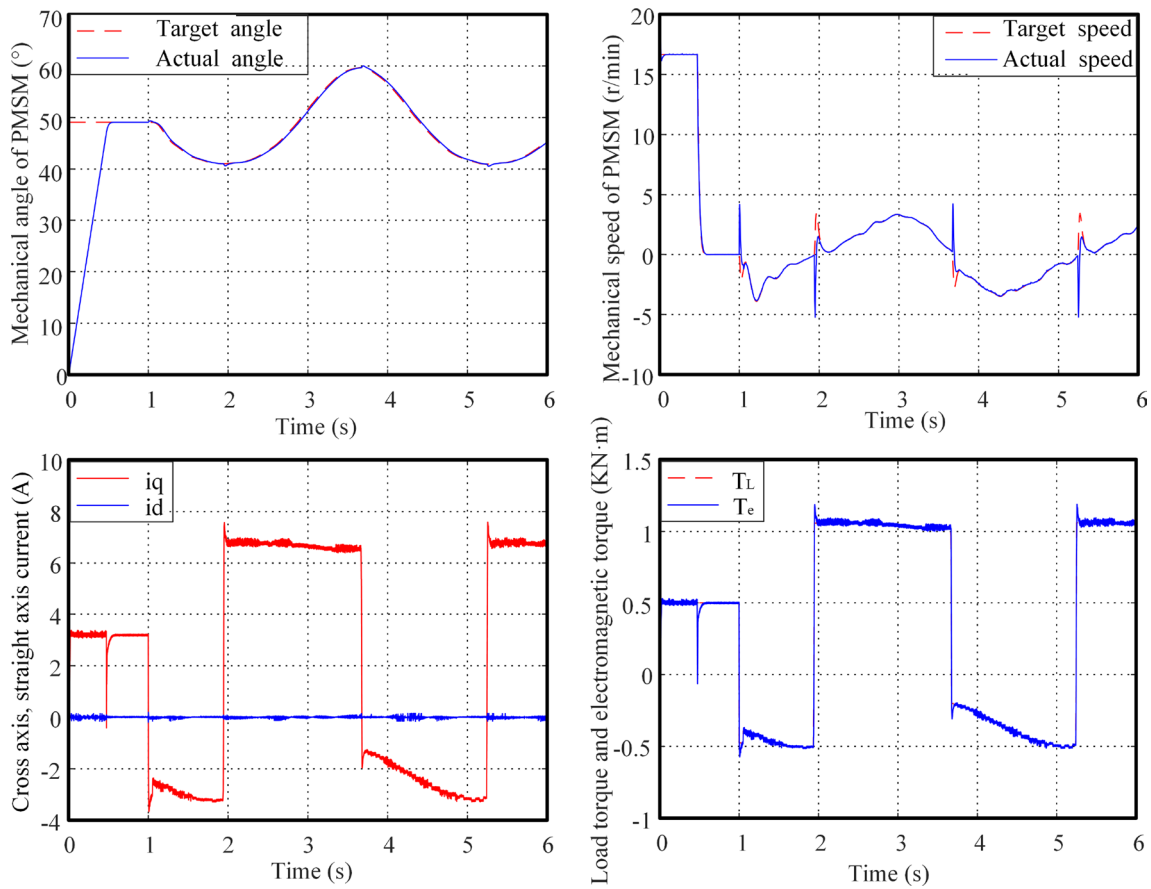


Fig. 7 Pitch angle position following control simulation curve

a good consistency with the target rotation angle. Since the electromagnetic torque T_e cannot respond to the load T_L in response to the speed, the motor speed fluctuates for a very

short time, but this has little effect on the motor position control accuracy. It can be seen that the position tracking effect based on the speed controller is better.

5 Experimental Verification and Discussions

To further observe the effectiveness of the proposed control method in practical application, the corresponding experimental research is carried out. The change frequency of pitch angle position command is low, which does not have high requirements on the bandwidth of the position controller, but there is a sudden load in the pitch process, and the sudden load will cause the fluctuation of the speed. If the speed controller cannot quickly suppress the fluctuation, the integral of the speed fluctuation with time will bring a rotation angle deviation that cannot be ignored to the system. It can be seen that the speed controller is the most critical of the three closed-loop controllers in the PMSM position control system. Therefore, this section mainly conducts speed control experiments under step load. The permanent magnet direct-drive variable-pitch simulation experiment platform is shown in Fig. 8, which is mainly composed of a PMSM, a coupling, a torque sensor, and a magnetic powder dynamometer. The blade load is simulated by the magnetic powder dynamometer.

The target speed of the motor is set to 15r/min. After the speed is stable, a step signal of 1000 N m is applied through the magnetic particle dynamometer. Since the magnetic particle dynamometer cannot produce negative torque, the negative step is simulated by removing the load of 1000 N m torque signal, after the motor is unloaded and the speed is stable, it will stop freely. The experimental data during the experiment is read by the host computer, and the experimental curves of speed, load, and current are shown in Fig. 9.

Through the experimental curve, it can be found that after starting the drive, the motor speed responds quickly and reaches the target speed. There is almost no overshoot in the speed, and there is a sinusoidal fluctuation after the motor reaches the rated speed. After loading, the speed drops and then quickly returns to the target speed. At this time, the motor response trend is similar to the simulation curve trend; when the unloading speed of the motor suddenly increases, it also quickly recovers; when the free stop is stopped, the motor speed tends to oscillate to zero

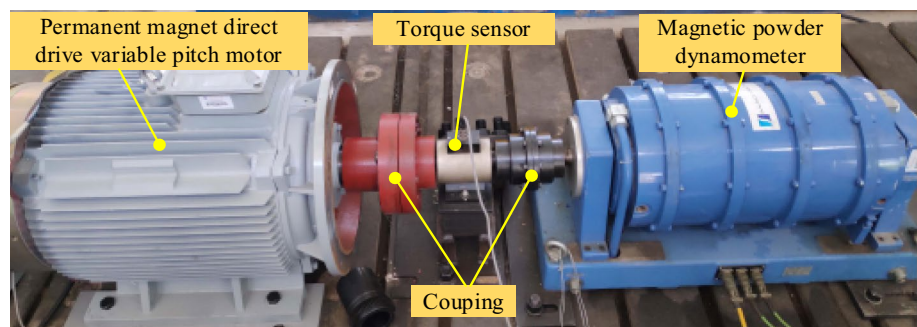
speed. It can be seen that the speed controller has a good suppression effect on the speed fluctuation caused by the sudden load, and basically meets the control requirements.

In order to further investigate the reason of the speed fluctuation of the motor in the steady state, the FFT transformation is performed on the speed and current in the steady state, and the spectrum chart is shown in Fig. 10. In steady state, the motor speed is 15r/min, which is converted to electrical angle frequency $f_e = 3$ Hz. There are two harmonic components of 2.93 Hz and 18.07 Hz in the speed spectrum chart, which are 1 times f_e and 3 times f_e , respectively. According to the number of motor slots and the number of pole pairs, the harmonic component of 18.07 Hz comes from the cogging torque ripple. The 2.93Hz harmonic component is probably caused by the asymmetry of the winding, which causes the motor torque to fluctuate periodically with f_e . There are also two harmonic components of 2.93 Hz and 18.07 Hz in the spectrum diagram of torque current i_q . The phase difference of the harmonics of the speed and torque current at 18.07 Hz is calculated by the cross-correlation function. It is found that the speed harmonic phase leads the current i_q about 113° . It can be seen that the torque ripple frequency of the PMSM is high, and the speed controller has a tendency to suppress the torque ripple, but it cannot completely suppress the torque ripple. However, due to the small amplitude and high frequency of the harmonic component of the rotating speed, the effect on the position control accuracy after integration is within the allowable range of the pitch angle error. It can provide a reference for further optimization of the speed controller.

6 Conclusion

This paper proposes a variable-pitch drive system for wind turbines driven by PMSM. In view of the abrupt changes in the pitch load of wind turbines, the control strategy of individual variable-pitch systems for wind turbines driven by PMSM is studied. Based on the LADRC control principle, a linear auto-disturbance speed controller and an extended observer are designed. A speed simulation model is built

Fig. 8 Physical diagram of the permanent magnet direct-drive pitch simulation experiment platform



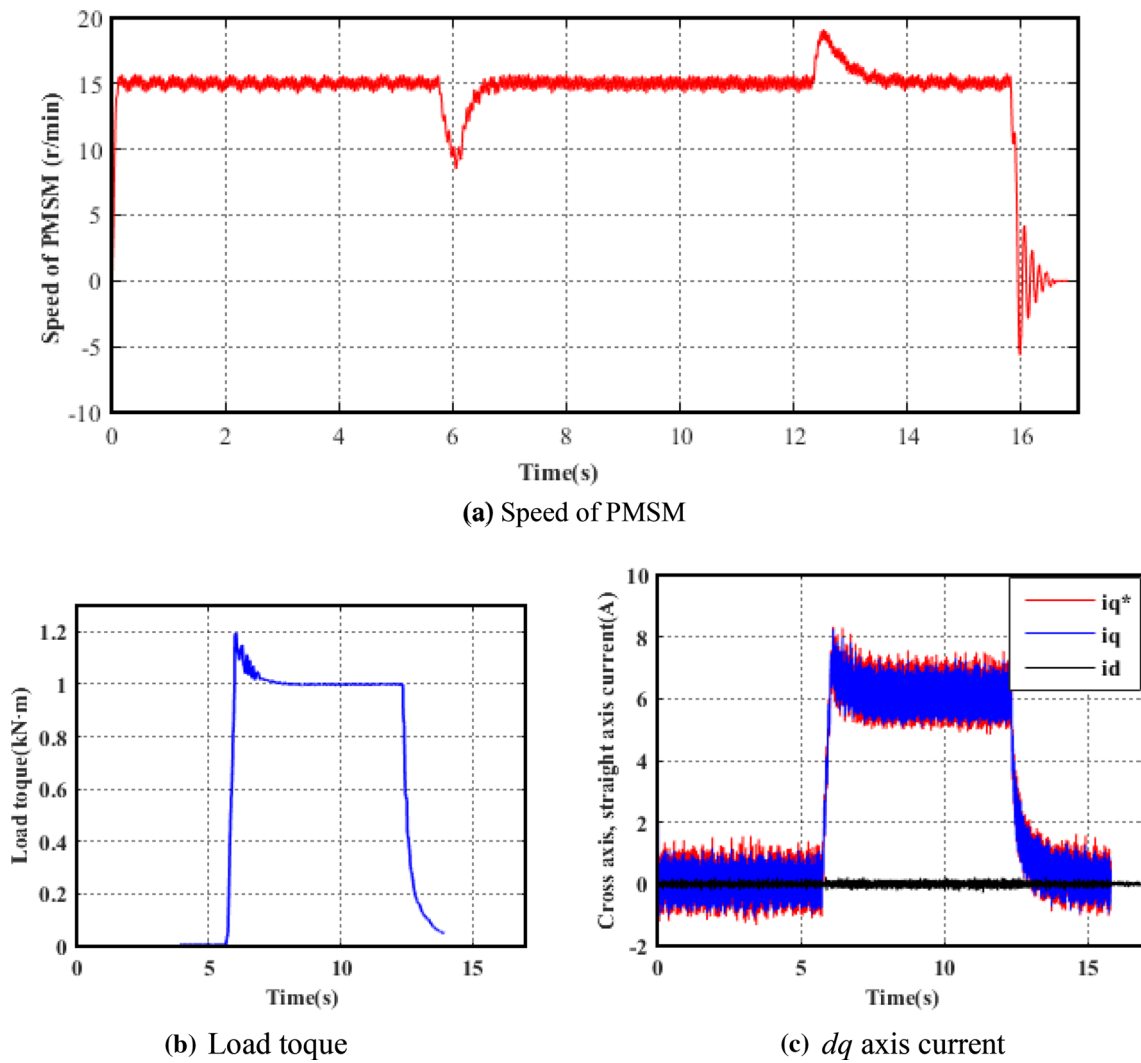


Fig. 9 Speed response experiment curve of permanent magnet direct-drive variable pitch motor. a Speed of PMSM, b Load torque, c dq axis current

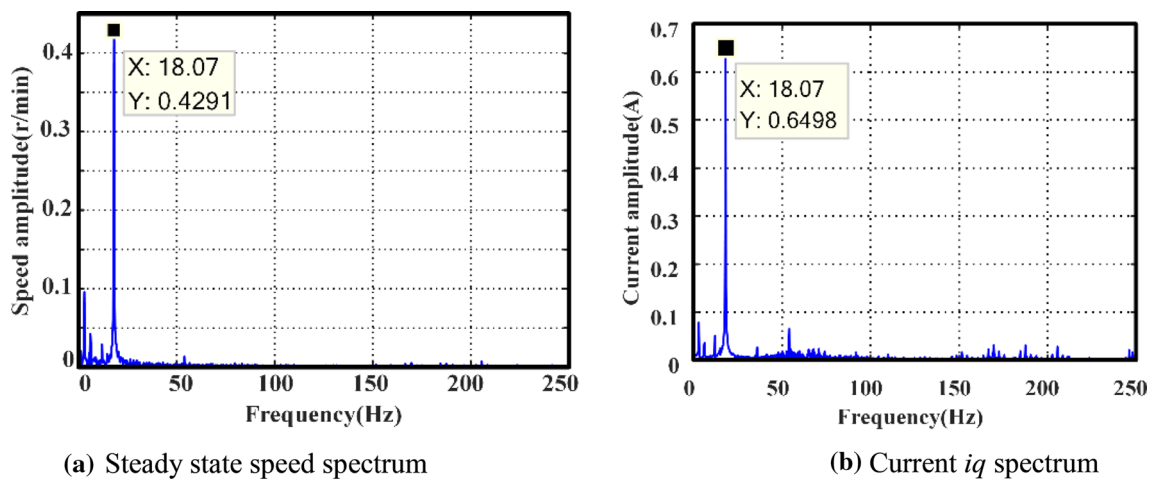


Fig. 10 Speed and q -axis current spectrum. a Steady state speed spectrum b Current i_q spectrum

using Matlab/Simulink, and an individual variable-pitch semi-physical simulation experiment platform is also built. The response performance of the system under sudden load is verified, and the reason for the fluctuation of the motor speed is analyzed. The simulation results show that the designed controller can meet the requirements of pitch angle position follow-up control, and it shows good robustness against the sudden change of pitch load. The individual variable pitch controller designed based on this speed controller has a good position tracking effect. The experiment shows that the semi-physical simulation experiment platform can simulate the variable-pitch drive experiment. The research results can provide a reference for further optimization of the speed controller and the construction of the load simulation platform.

Although the controller has good control effect at present, the phenomenon of instantaneous loss of rotation still exists when the load changes suddenly. In future work, the relevant control algorithms such as sliding mode control and adaptive control will be combined to further optimize the pitch control.

Acknowledgements This work is supported by the National Natural Science Foundation of China (Grant No.52005232,51775543), National Natural Science Foundation of Jiangsu Province, China (Grant No.BK20201024), the Natural Science Foundation of Jiangsu Normal University, China (Grant No. 19XSRX016) and the Key Research and Development Project of Xuzhou (Grant No. KC17014).

Compliance with ethical standards

Conflicts of interest The authors declare no conflict of interest.

References

- Liu W, Ren H (2020) A novel wind turbine health condition monitoring method based on common features distribution adaptation. *Int J Energy Res* 44(11):8681–8688
- Liu WY, Tang BP, Han JG, Lu XN, Hu NN, He ZZ (2015) The structure healthy condition monitoring and fault diagnosis methods in wind turbines: A review. *Renew Sustain Energy Rev* 44:466–472
- Magar KT, Balas MJ, Frost S (2015) Direct adaptive control for individual blade pitch control of wind turbines for load reduction. *J Intell Mater Syst Struct* 26(12):1564–1572
- van Solingen E, Fleming PA, Scholbrock A, van Wingerden JW (2016) Field testing of linear individual pitch control on the two-bladed controls advanced research turbine. *Wind Energy* 19(3):421–436
- Jin X, Wang Y, Li L (2016) Dynamics loads optimization analysis of wind turbine based on LQG independent pitch control. *Proc CSEE* 36(22):6164–6170
- Zhang Y, Chen Z, Hu W, Cheng M (2014) Flicker mitigation by individual pitch control of variable speed wind turbines With DFIG. *IEEE Transac Energy Conver* 29(1):20–28
- Liu X, Yu W, Yang L and Ma Q (2017) Research on variable-pitch control strategy of wind turbine based on the nonlinear PID. In: 2017 Chinese Automation Congress (CAC) (pp. 299–303). IEEE.
- Xie B, Wang S, Wang Y, Zhao Z, Xiu J (2015) Magnetically induced rotor vibration in dual-stator permanent magnet motors. *J Sound Vibr* 347:184–199
- Zhou Y, Li H, Zhang H (2018) Model-free deadbeat predictive current control of a surface-mounted permanent magnet synchronous motor drive system. *J Power Electr* 18(1):103–115
- Usop Z, Sarhan AAD, Mardi NA, Wahab MNA (2015) Measuring of positioning, circularity and static errors of a CNC Vertical Machining Centre for validating the machining accuracy. *Measurement* 61:39–50
- Zi B, Sun H, Zhang D (2017) Design, analysis and control of a winding hybrid-driven cable parallel manipulator. *Robot Comput-Integr Manufac* 48:196–208
- Chen X, Wei H, Deng T, He Z, Zhao S (2018) Investigation of electromechanical coupling torsional vibration and stability in a high-speed permanent magnet synchronous motor driven system. *Appl Math Modell* 64:235–248
- Nerg J, Rilla M, Ruuskanen V, Pyrhoenen J, Ruotsalainen S (2014) Direct-driven interior magnet permanent-magnet synchronous motors for a full electric sports car. *IEEE Transac Industr Electr* 61(8):4286–4294
- Ren J-J, Liu Y-C, Wang N, Liu S-Y (2015) Sensorless control of ship propulsion interior permanent magnet synchronous motor based on a new sliding mode observer. *ISA Transac* 54:15–26
- Lu E, Li W, Yang X, Xu S (2017) Composite sliding mode control of a permanent magnet direct-driven system for a mining scraper conveyor. *IEEE Access* 5:22399–22408
- Sheng L, Li W, Wang Y, Fan M, Yang X (2017) Sensorless control of a shearer short-range cutting interior permanent magnet synchronous motor based on a new sliding mode observer. *IEEE Access* 5:18439–18450
- Wallmark O, Harnefors L, Carlson O (2007) Control algorithms for a fault-tolerant PMSM drive. *IEEE Transac Industr Electron* 54(4):1973–1980
- Bossanyi EA (2003) Individual blade pitch control for load reduction. *Wind Energy* 6(2):119–128
- Sandquist F, Moe G, Anaya-Lara O (2012) Individual pitch control of horizontal axis wind turbines. *J Offshore Mechan Arctic Eng* 134(3):031901
- Liu H, Tang Q, Chi Y, Zhang Z, Yuan X (2016) Vibration reduction strategy for wind turbine based on individual pitch control and torque damping control. *Int Transac Electr Energy Syst* 26(10):2230–2243
- Ren Y, Li L, Brindley J, Lin J (2016) Nonlinear PI control for variable pitch wind turbine. *Control Eng Pract* 50:84–94
- Tan Luong V, Thanh Hai N, Lee D-C (2015) Advanced pitch angle control based on fuzzy logic for variable-speed wind turbine systems. *IEEE Transac Energy Conv* 30(2):578–587
- Asgharnia A, Shahnazi R, Jamali A (2018) Performance and robustness of optimal fractional fuzzy PID controllers for pitch control of a wind turbine using chaotic optimization algorithms. *ISA Transac* 79:27–44
- Yin XX, Lin YG, Li W, Liu HW, Gu YJ (2015) Adaptive sliding mode back-stepping pitch angle control of a variable-displacement pump controlled pitch system for wind turbines. *ISA Transac* 58(5):629–634
- Lasheen A, Elnaggar M, Yassin H (2019) Adaptive control design and implementation for collective pitch in wind energy conversion systems. *ISA Transac* 102:251–263
- Yuan Y, Tang J (2017) Adaptive pitch control of wind turbine for load mitigation under structural uncertainties. *Renew Energy* 105:483–494

27. Wang Y, Jiang B, Wu Z, Xie S, Peng Y (2020) Adaptive sliding mode fault-tolerant fuzzy tracking control with application to unmanned marine vehicles. *IEEE Transac Syst, Man, Cybern: Syst.* <https://doi.org/10.1109/TSMC.2020.2964808>
28. Wang Y, Xie X, Chadli M, Xie S, Peng Y (2020) Sliding mode control of fuzzy singularly perturbed descriptor systems. *IEEE Transac Fuzzy Syst.* <https://doi.org/10.1109/TFUZZ.2020.2998519>
29. Liu L, Liu YJ, Chen A, Tong S, Chen CP (2020) Integral Barrier Lyapunov function-based adaptive control for switched nonlinear systems. *Sci China Info Sci* 63(3):212–225
30. Liu L, Liu Y-J, Li D, Tong S, Wang Z (2020) Barrier Lyapunov function-based adaptive fuzzy ftc for switched systems and its applications to resistance-inductance-capacitance circuit system. *IEEE Transac Cybern* 50(8):3491–3502
31. Tang L, Ma D, Zhao J (2019) Adaptive neural control for switched non-linear systems with multiple tracking error constraints. *IET Signal Process* 13(3):330–337

Publisher's Note Springer Nature remains neutral with regard to jurisdictional claims in published maps and institutional affiliations.

Lianchao Sheng received the B.E. and Ph.D. degree from the School of Mechatronic Engineering, China University of Mining and Technology, Xuzhou, China, in 2014 and 2019, respectively. Since 2019, he

became a lecturer in the School of Mechanical and Electrical Engineering, Jiangsu Normal University. His research interests include control algorithm and nonlinear dynamics analysis of electromechanical transmission system.

Min Li received the B.E. degrees from the School of Mechatronic Engineering, China University of Mining and Technology, Xuzhou, China, in 2020. His current research interests include control algorithm and electromechanical dynamics of wind power generator.

Yueqi Li is currently studying in the school of mechanical and electrical engineering, Jiangsu Normal University. Her research interests include control algorithm and nonlinear dynamics analysis of electro-mechanical transmission system.

Wei Li received the M.E. and Ph.D. degrees from the China University of Mining and Technology, Xuzhou, China, in 1989 and 2004, respectively. He is now a professor at School of Mechatronic Engineering with the China University of Mining and Technology. His research interests include control algorithm, electromechanical coupling dynamics, coordinated positioning of moving targets, etc.